Available online at www.sciencedirect.com
ScienceDirect
Trans. Nonferrous Met. Soc. China 35(2025) 1758−1771
Transactions of Nonferrous Metals Society of China
www.tnmsc.cn

Statistical analysis of anomalous tension twin and twin transmission in pure Mg sheet for various grain sizes and strain rates

Sai-jun HUANG[1], Ran NI[1], You-fu WAN[1], Hao ZHOU[2], Ying ZENG[1], Dong-di YIN[1]

1. Key Laboratory of Advanced Technologies of Materials, Ministry of Education, School of Materials Science and Engineering, Southwest Jiaotong University, Chengdu 610031, China;
2. Nano and Heterogeneous Materials Center, School of Materials Science and Engineering, Nanjing University of Science and Technology, Nanjing 210094, China

Received 7 October 2023; accepted 28 April 2024

Abstract: A statistical analysis of the twinning behavior in a basal-textured Mg sheet under hard orientation loading was performed at strain rates of 1×10^{-5} and 1×10^{-1} s^{-1} with grain sizes of 70 and 20 μm. There were 1609 tension twins identified including adequate (51%) anomalous twins (Schmid factor m<0). Twin variant selection exhibited almost no grain size or strain rate effects. Most twin variants (74%) correlated well with the proposed normalized Schmid factor (m_{nor}). The Luster−Morris parameter (m') values failed to correlate with the twin transmission, while 96% of transmitted pairs exhibited large m_{nor} or normalized m' (m'_{nor}) values. Twin transmission occurred more frequently at lower grain boundary misorientation angles (10°−30°). The active anomalous twins correlated well with m of the prismatic slip. The present work provided a statistical perspective that, the m_{nor} and m'_{nor} can correlate the anomalous twinning rather than m and m'. The local condition also played a critical role in anomalous twinning behavior.
Key words: Mg; anomalous twin; twin transmission; Schmid factor; Luster−Morris parameter

1 Introduction

As the lightest structural metal, magnesium (Mg) alloys have attracted considerable interest in the aerospace, railway, automotive and other industries [1−4]. However, due to their close-packed hexagonal (HCP) crystal structure, Mg alloys displayed intricate mechanical behavior [5,6].

Deformation twinning plays an important role in the plastic deformation of Mg and its alloys [7,8]. Among various twinning modes, $\{10\bar{1}2\}$ tension twin (TTW) exhibits notably lower critical resolved shear stress (CRSS) and is the most prevalent twinning mode during plastic deformation [9−11]. However, the twinning activity is polar [12−15]. It is well-accepted that the formation of twinning is a complex phenomenon influenced by various factors, such as temperature [16], strain rate [17,18], and grain size [19]. It is noteworthy that while most of the above works have primarily focused on the activity of twinning, the twin variant selection has been less investigated. Therefore, detailed statistical analysis on the twin variant selection of pure Mg at different strain rates and grain sizes is essential to obtain a more comprehensive understanding of twinning behavior.

Schmid factor (m) is a widely employed geometric parameter that is correlated with the activity of twinning. Although the accuracy of m has been validated in numerous experiments [20,21], several studies have still observed the activation of

Corresponding author: Dong-di YIN, Tel: +86-28-87634673, E-mail: ahnydd@swjtu.edu.cn;
Ying ZENG, E-mail: clzy@swjtu.edu.cn
https://doi.org/10.1016/S1003-6326(25)66781-1

twins with low or even negative *m* values, i.e. anomalous twins [22,23]. CHAI et al [24] found that pure Mg under hard orientation activated a high percentage of anomalous TTW. More recently, based on a statistical analysis of TTWs in basal textured polycrystalline Mg, Zr and Ti, KUMAR and BEYERLEIN [25,26] proposed that the nucleation, growth, and proliferation of deformation twinning in HCP metals are stochastic, which was supported by modeling incorporated in the stochastic twin model. Thus, a detailed statistical investigation of twinning, which is introduced in this work, is crucial.

It is worth noting that the above results were obtained with soft orientation loading for TTW, i.e. compression along the extrusion direction (ED) for basal textured polycrystals. However, the understanding of twinning behavior under hard orientation loading of TTW (tension along the ED) remains inadequate. During the hard orientation loading, some researchers [27] reported expected CTWs with large *m* values, while others observed high activity of TTWs with negative *m* values (anomalous TTWs) [28,29]. JONAS et al [27] investigated twinning activity in extruded and textured AM30 and AZ31 during ED tension. Many expected CTWs and CTW-TTW double twins were observed. In contrast, some unexpected anomalous TTWs with negative *m* values in hot-rolled pure Mg during compression along the normal direction (ND) in a channel die have been identified by NAVE and BARNETT [29].

Therefore, the detailed investigation on twinning activity, variant selection, and twin transmission for polycrystalline Mg with various grain sizes under hard orientation loading at various strain rates and grain sizes based on large data sets, has statistical significance for further understanding of deformation twinning. In this work, the twinning behavior of pure Mg sheets with average grain size of 20 and 70 μm under tension along the ED at strain rates of 1×10^{-1} and 1×10^{-5} s^{-1} was quantitatively investigated using electron back-scatter diffraction (EBSD). From a statistical perspective, a significant number of anomalous TTW twins were studied and compared to gain insights into their activation mechanisms. Furthermore, twin transmission in the hard orientation is also statistically analyzed to examine the possible correlations to *m′*, *m* and grain boundary misorientation angle (GBMA), under various strain rates and grain size conditions.

2 Experimental

The material studied in this work was prepared from high-purity Mg (99.9%) by extrusion after steel mold casting. More details of the extrusion processing of the material can be found in our previous studies [30−32]. Then, the as-extruded pure Mg was annealed at 350 °C for 25 s or 1.5 h and immediately quenched in water to obtain the target material with average grain sizes of 20 or 70 μm, respectively.

The microstructures of the annealed sheet were characterized on the ED−transverse direction (TD) plane using electron backscatter diffraction (EBSD, Oxford Instrument Nordlys Nano) measurements in a field emission scanning electron microscope (SEM, JEOL JSM−7800F). The sample surfaces were mechanically polished. More detailed procedures can be found in our previous work [33,34].

The bone-shaped specimens for tension had a gage length of 18 mm (parallel to ED), width of 3 mm (parallel to TD), and thickness of 2 mm (parallel to ND). Quasi-static uniaxial tensile tests were conducted at room temperature along the ED at various strain rates of 1×10^{-5} and 1×10^{-1} s^{-1} until fracture using a precision universal testing machine (MTS-CMT5105). For the twin analysis, all specimens were slightly re-polished after failure, and then the regions near the fracture surface of the samples were investigated using EBSD analysis. Each studied area consisted of 300−1000 grains. The step size for EBSD ranged from 0.5 to 2 μm according to different grain sizes, and the index ratio for all samples was above 90%. For the analysis of raw EBSD data and twin variants, a custom MATLAB code [32,34−36] based on the MTEX toolbox [37,38] was utilized.

3 Results

3.1 Initial microstructure

Figure 1 illustrates the initial microstructure of the extruded Mg in the ED−TD plane with different grain sizes, including EBSD inverse pole figure

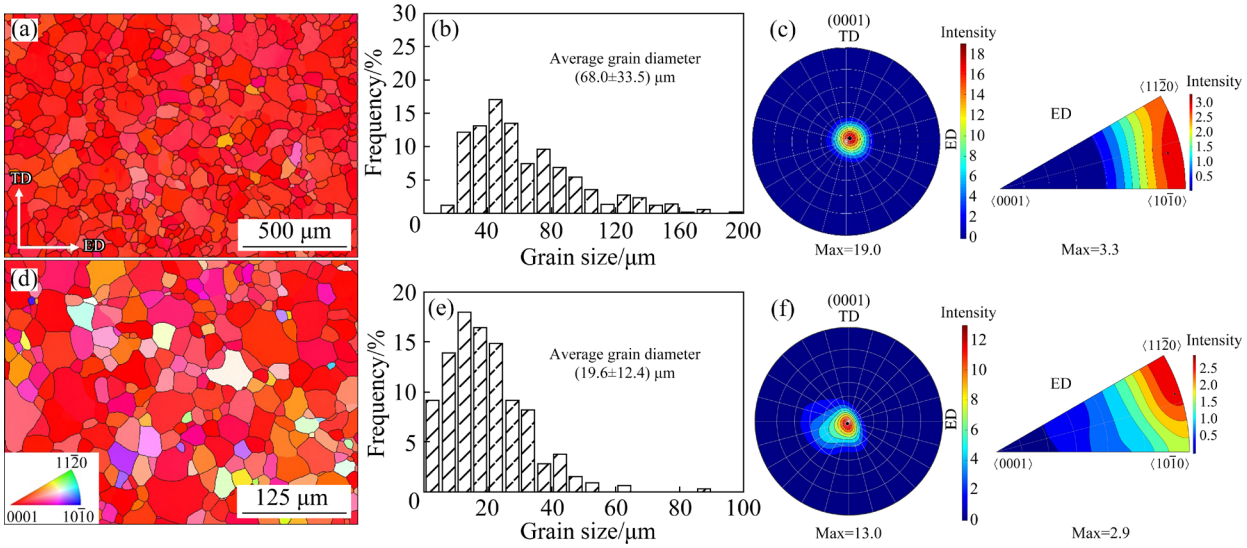

Fig. 1 Initial microstructure of Mg sheet in ED−TD plane with different grain sizes: (a−c) 70 μm; (d−f) 20 μm; (a, d) EBSD IPF along ND; (b, e) Equivalent grain diameter distribution; (c, f) {0001} PF and ED IPF

(IPF) maps, grain size distribution, {0001} pole figure (PF), and IPF along ED. As revealed by the IPF maps (Figs. 1(a) and (d)), the initial microstructure exhibits fully recrystallized uniform equiaxial grains. The distribution of grain size (equivalent circle diameter) for each sample is shown in Figs. 1(b) and (e), which suggested that the average grain sizes were (68.0±33.5) and (19.6±12.4) μm, respectively, and referred to as 70 and 20 μm for convenience. Pure Mg exhibited a strong basal texture as seen in Figs. 1(c) and (f). The peak intensity of {0001} PF was greater than 10 multiples random distribution (mrd), revealing that most of the grains' *c*-axis was nearly parallel to the ND. Besides, the ED IPF displayed a maximum pole intensity of ~3 mrd.

3.2 Deformed microstructure

A total of 1693 twins containing 1609 TTWs were recorded and analyzed in this work. Figure 2 presents the IPF maps and corresponding twin boundary maps of the pure Mg sheets in coarse grain (70 μm), tensioned to fracture at strain rates of 1×10^{-5} and 1×10^{-1} s^{-1}. The boundary map utilized various colors based on boundary misorientation analysis. At a high strain rate of 1×10^{-1} s^{-1}, a total of 485 twins were observed, all of which were TTWs (Figs. 2(a) and (c)). Likewise, at a low strain rate of 1×10^{-5} s^{-1}, a total of 583 twins were identified, including 532 TTWs and a minimal amount of CTW and DTW (Figs. 2(b) and (d)).

The IPF maps and twin boundary maps of 20 μm pure Mg after failure at different strain rates are shown in Fig. 3. At a high strain rate of 1×10^{-1} s^{-1}, a total of 276 twins were identified, including 261 TTW and a few CTW and DTW (Figs. 3(a) and (c)). Similarly, at a low strain rate of 1×10^{-5} s^{-1}, a total of 349 twins were analyzed, consisting of 331 TTW and negligible CTW or DTW (Figs. 3(b) and (d)). Since almost all twins were TTW, which was independent of grain size and strain rate, the term "twins" used subsequently refers to TTW unless otherwise specified.

3.3 Twinning activity

To investigate the activation of twinning, Fig. 4 shows the method of the twin variant analysis. Figure 4(a) illustrates the IPF map of the parent grain 694 (the grain was labeled 694) and its five twin variants. Different twin modes can be directly determined from EBSD boundary misorientation analysis based on the theoretical twin-parent misorientation relationships with maximum deviation of 10°. For the grain 694, each of the five twins was identified as TTW. The first row of Fig. 4(b) presents the orientation of parent grain 694 obtained by EBSD. Based on the rotation relationship between the parent grain and twins [8], i.e. rotating 180° around the twinning direction η_1 in the crystallographic coordinates of parent grain, the orientations of six theoretical twin variants with corresponding *m* values for each variant assuming that the stress state of each grain is consistent with the macroscopic applied stress were calculated based

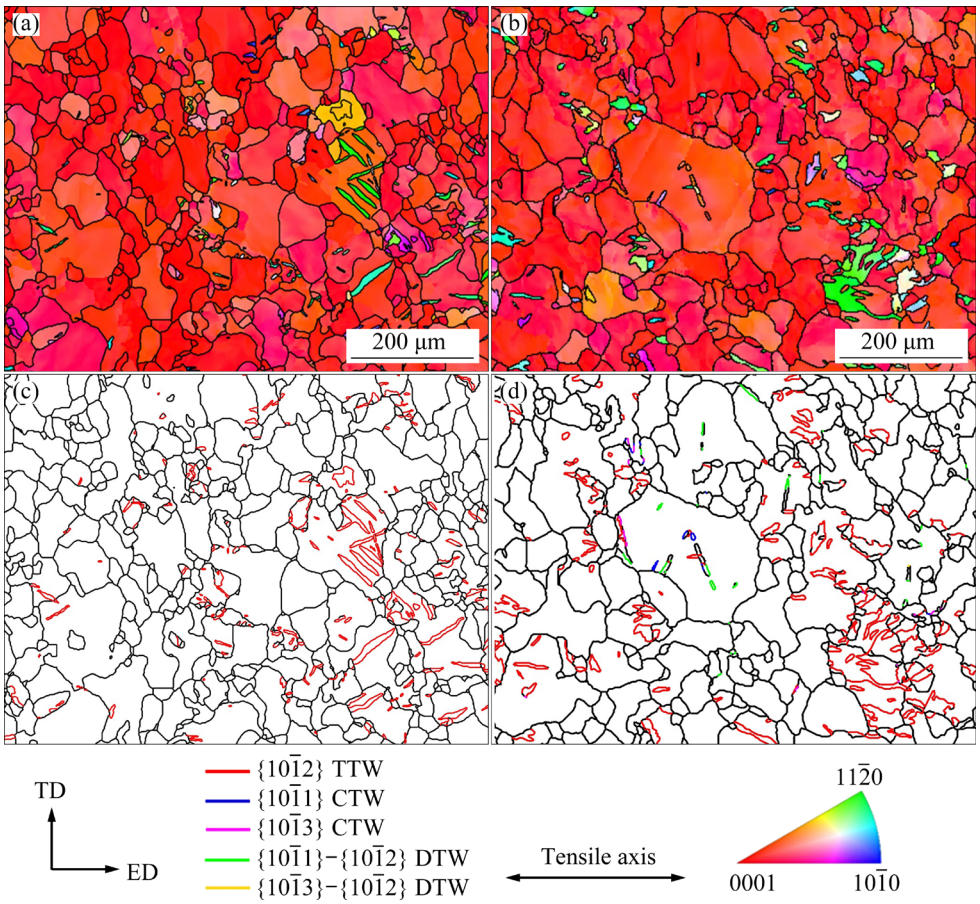

Fig. 2 Microstructure of 70 μm Mg after failure at strain rates of 1×10^{-1} s^{-1} (a, c) and 1×10^{-5} s^{-1} (b, d): (a, b) IPF map; (c, d) Corresponding boundary map illustrating twinning activity

on MTEX [37,38], as shown in the second row of Fig. 4(b). The third row of Fig. 4(b) illustrates the orientation deviation between the observed twin and the six theoretical variants, which was used to identify the activated twin variant. It was determined that the five TTWs activated in grain 694-P were identified as 682-V2, 665-V3, 729-V4, 702-V5, and 683-V6, with corresponding m values of −0.21, −0.01, −0.41, −0.19, and −0.02, respectively.

A significant number of anomalous twins were activated in pure Mg with various grain sizes after tension to fracture at different strain rates. Twin variant selection exhibited similar trends for different grain sizes or strain rates. Figure 5 presents the distribution and relative frequencies of the m and m_{nor} of the activated TTWs identified in all samples. As depicted in Fig. 5(a), the m values were predominantly distributed in the range of −0.2 to 0.2, with 51% anomalous twins ($m<0$) being activated. Evidently, m failed to correlate the twin variant selection under the current hard orientation loading. Therefore, we proposed a normalized Schmid factor (m_{nor}), and defined it as follows [32]:

$$m_{nor}=(m-m_{min})/[2(m_{max}-m_{min})] \quad (1)$$

The m_{nor} was employed to estimate the proximity of the activated m to the maximum m among the theoretically proposed six variants. A higher m_{nor} indicates a smaller difference of the m with m_{max}. As depicted in Fig. 5(b), the m_{nor} values tended to distribute from 0.45 to 0.5, with 74% of the twin variants exhibiting $m_{nor}>0.4$, while 10% of the variants had $m_{nor}<0.1$. Despite the substantial TTWs with $m<0$, most m values were close to m_{max}, thus highlighting the potential of m_{nor} in helping the TTW variant selection.

When twins propagate to grain boundaries, they could trigger the nucleation and growth of another twin in adjacent grains, which is referred to as twin transmission [25,39]. Twin transmission serves as a crucial mechanism for accommodating intergranular deformation at grain boundaries. The potential of twin transmission was commonly

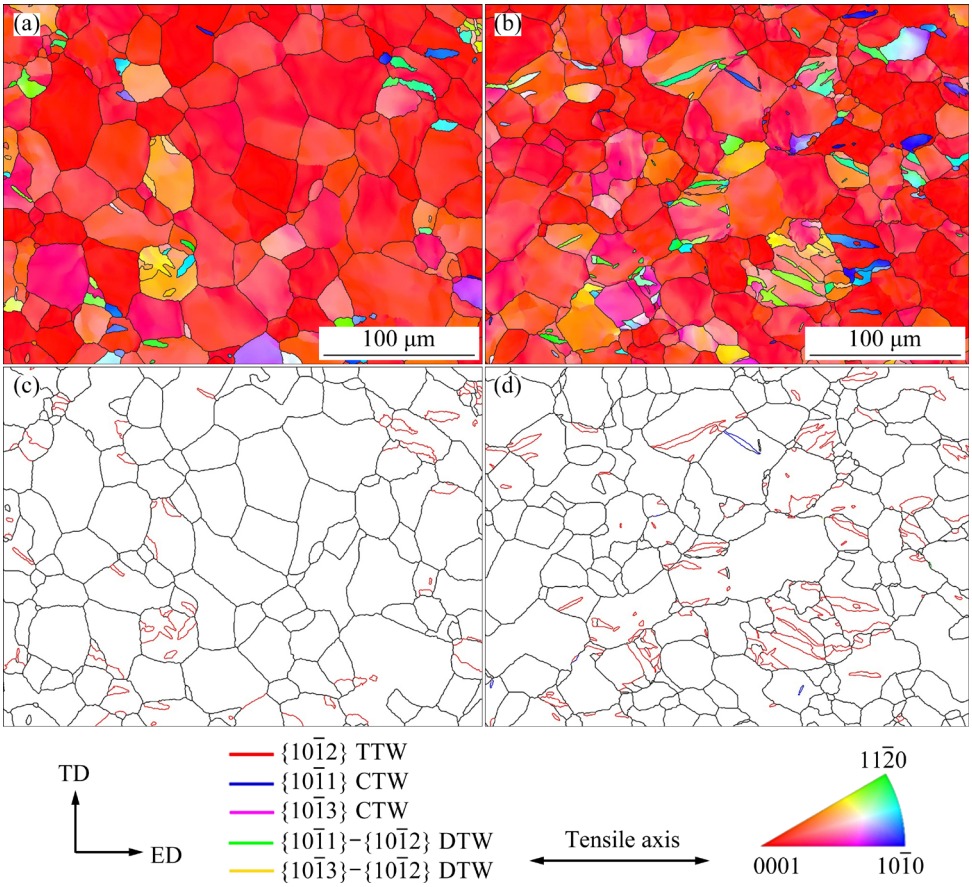

Fig. 3 Microstructure of 20 μm Mg after failure at strain rates of 1×10^{-1} s^{-1} (a, c) and 1×10^{-5} s^{-1} (b, d): (a, b) IPF map; (c, d) Corresponding boundary map illustrating twinning activity

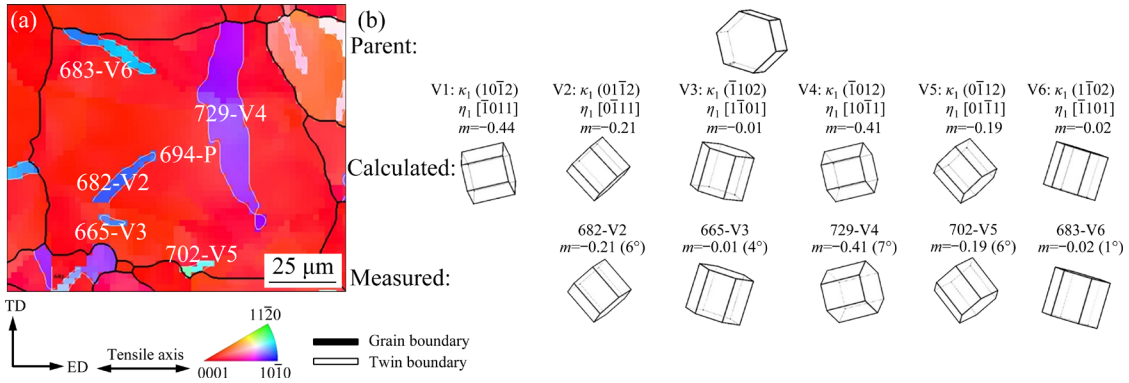

Fig. 4 Illustration of twin variants identification procedure in grain 694: (a) IPF map of grain 694-P containing five twins; (b) Parent grain orientation, calculated twin variants containing crystallographic orientation, and measured twin variants orientation

characterized by Luster−Morris parameter (m') that was obtained using the following formula [40]:

$$m'=\cos\kappa\cos\psi \tag{2}$$

where κ and ψ represent the angle between the twinning planes and the twinning shear directions of the two twinning systems, respectively. Three representative twin transmissions are illustrated in Fig. 6. Similar to the normalization method for the m described earlier, a normalized m' was introduced and defined as follows [33]:

$$m'_{nor}=(m'-m'_{min})/(m'_{max}-m'_{min}) \tag{3}$$

This parameter evaluates the proximity between the activated m' and the maximum $m'(m'_{max})$. The larger the m'_{nor} is, the closer the m' is to m'_{max}.

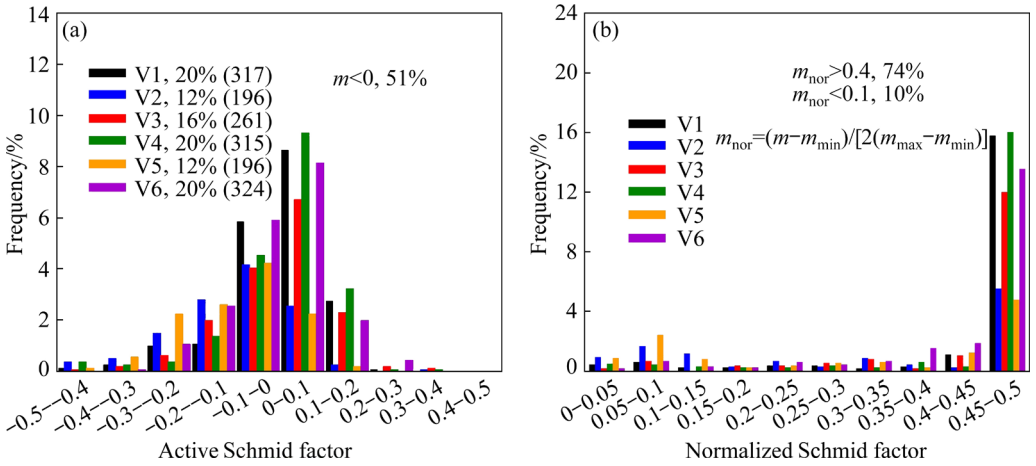

Fig. 5 Distribution of Schmid factor (m) (a), and normalized Schmid factor (m_{nor}) (b) of all TTWs

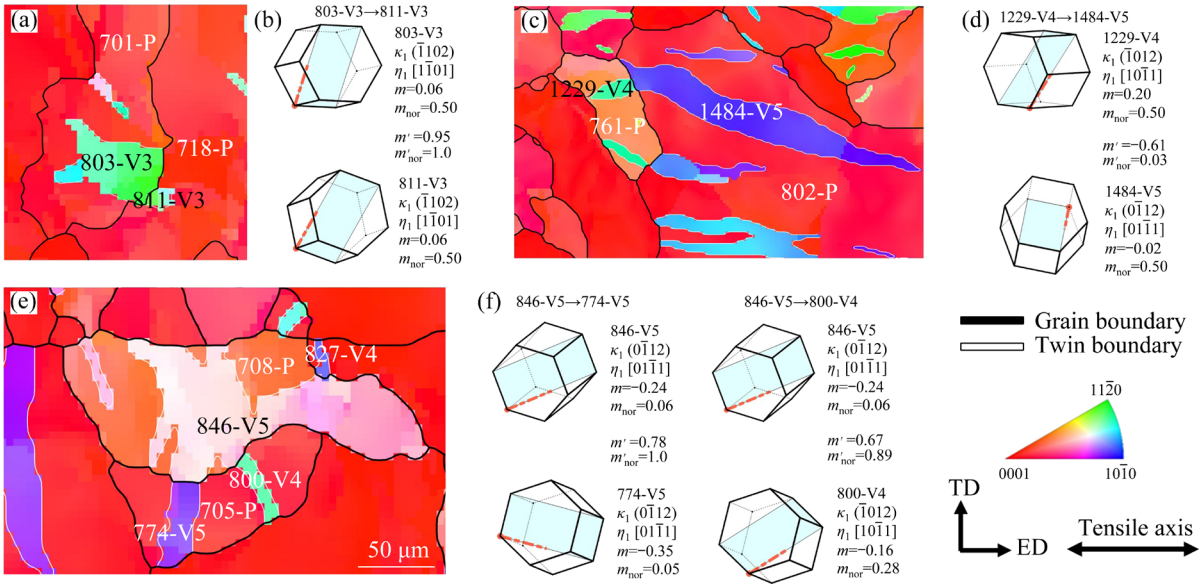

Fig. 6 Representative example of twin transmission: (a, c, e) IPF maps; (b, d, f) Twinning plane κ_1, twinning direction η_1 and geometric parameters, respectively

Figure 6(a) illustrates an example between the twins labeled as 803-V3 and 811-V3, accompanied by visual representations of corresponding active twinning systems in the HCP unit cell, m and m' (Fig. 6(b)). While both 803-V3 and 811-V3 had the highest m value (0.06) among the six possible variants (m_{nor}=0.50). The corresponding m' value (0.95) for the transmitted pair was also maximal (m'_{nor}=1.0), indicating good geometric compatibility for this transmitted pair. Additionally, the cases where the m or m' values for twin transmissions were not high also occurred, even after being normalized (Figs. 6(c−f)). The 1229-V4 and 1484-V5 twins were connected at grain boundary which exhibited the highest m_{nor} values although 1484-V5 had m < 0 (−0.02), while the m' and m'_{nor} values of them were low. Therefore, in some instances, the m may be more important than the m'. Figures 6(e) and (f) demonstrate two twin transmissions. For twins 846-V5 and 774-V5, 846-V5 had a negative m value (−0.24), and 774-V5 also had a small m. Therefore, the activation of these twins was not a response to the global stress. The large values of m' (0.78) and m'_{nor} (1.0) for the transmission pair indicate good geometric compatibility between the two twinning systems. The twin pair 846-V5 and 800-V4 had a relatively high m' but presented small m values. It is considered that the m' plays a more significant role than the m. Therefore, under the given loading conditions, neither the individual m nor m' can effectively correlate twin transmission [24].

To further understand the effect of strain rate and grain size on twin transmission, quantitative

statistics are presented in Fig. 7. A total of 343 transmitted twins were observed in 1609 twins. Figures 7(a) and (b) respectively illustrate the proportions of transmitted twins and the occurrence of boundaries connected to at least one transmitted twin pair. As the strain rate decreased, the proportion of twin transmission at 20 μm rose from 22% to 24%, while the proportion of transmitted grain boundaries increased from 2% to 3%. For 70 μm pure Mg, the influence of strain rate on the proportion of twin transmission appeared to be more pronounced, with the proportion increasing from 17% to 24%, while the transmitted grain boundary fraction rose from 1% to 4%. The above results revealed that, for pure Mg under the present hard orientation loading, the proportion of twin transmission increased as the strain rate decreased.

For investigating the influence of m and m' on twin transmission further, we plotted the distribution of transmitted twins as m'–m_1–m_2 heatmaps (Fig. 8), where m_1 represents the m of the thicker twin, and m_2 represents the m of the thinner

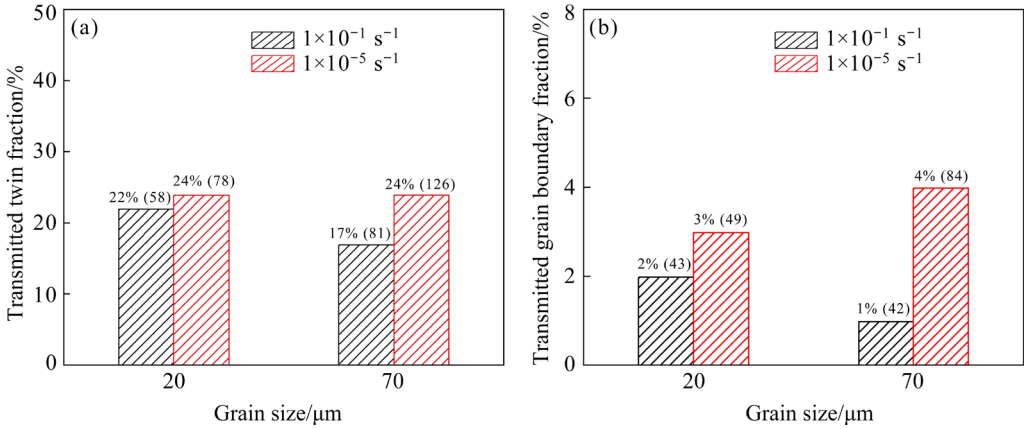

Fig. 7 Fraction of twin transmission for different grain sizes and strain rates: (a) Fraction of transmitted twins; (b) Occurrence of boundaries connected to at least one transmitted twin pair

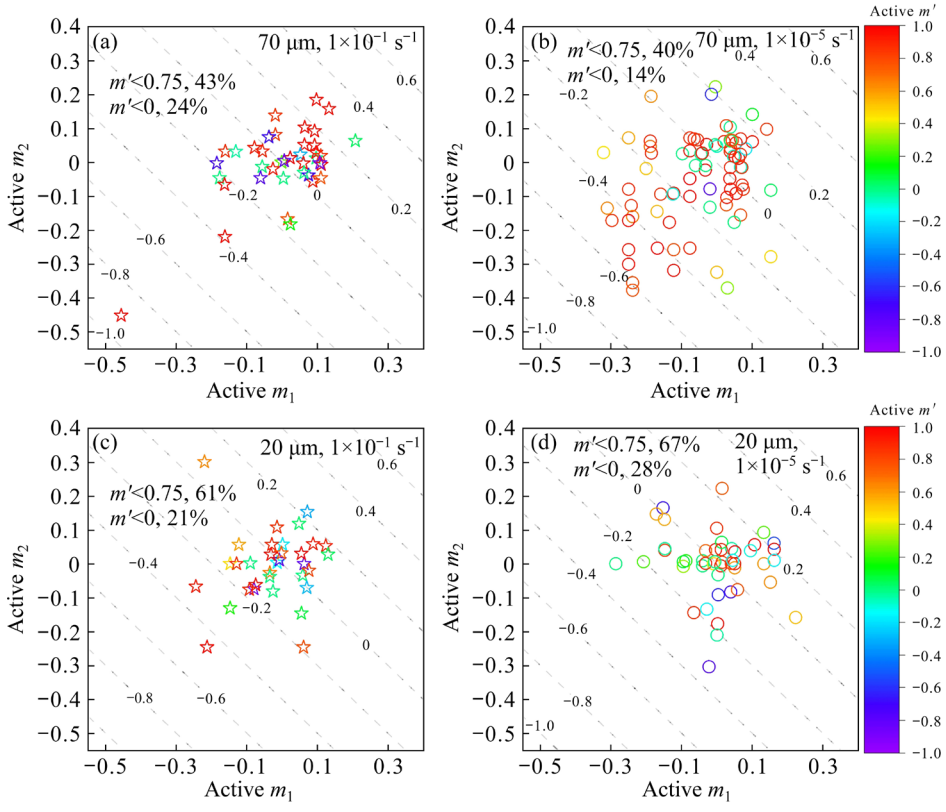

Fig. 8 Distributions of transmitted pairs in m'–m_1–m_2 heatmap for different grain sizes and strain rates

twin. The m' values were distributed within a range of −1 to 1. As shown in Fig. 8(a), for coarse-grain (70 μm) Mg at a high strain rate of 1×10^{-1} s^{-1}, 43% of the transmitted pairs exhibited $m'<0.75$, and 24% of them exhibited $m'<0$. Similarly, at a low strain rate of 1×10^{-5} s^{-1}, 40% of transmitted pairs had $m'<0.75$, and 14% of them had $m'<0$ (Fig. 8(b)). Likewise, for fine-grain (20 μm) Mg at a high strain rate of 1×10^{-1} s^{-1}, 61% of transmitted pairs had $m'<0.75$, and 21% of them had $m'<0$ (Fig. 8(c)). At a low strain rate of 1×10^{5} s^{-1}, 67% of transmitted pairs had $m'<0.75$, and 28% of them had $m'<0$ (Fig. 8(d)). For different strain rates and grain sizes, about 50% of the transmitted twin pairs exhibited low m' values ($m'<0.75$), and ~20% of them exhibited even negative values.

Therefore, considering the normalization method described earlier, Fig. 9 displays the m'_{nor}–m_{nor1}–m_{nor2} heatmap. Similar patterns were observed for different strain rates and grain sizes. After normalization, around 58% of all the transmitted twins exhibited $m'_{nor}>0.8$, while approximately 31% of them had $m'_{nor}<0.5$. Moreover, for most transmitted pairs, at least one of the m_{nor} values approached the maximum value of 0.5, and 80% of transmitted pairs had $m_{nor1}+m_{nor2}>0.6$. When both m_{nor} and m'_{nor} were considered, nearly all transmitted pairs (~96%) had m_{nor} or m'_{nor} values approached the maximum values ($m'_{nor}>0.9$, $m_{nor}>0.45$), accounting for approximately 95% in the coarse-grained samples (70 μm) and approximately 98% in the fine-grained samples (20 μm).

Twin transmission appeared to be associated with grain boundaries [33,41−43]. Figure 10 illustrates the relationship between twin transmission and the GBMA. Transmitted pairs preferentially occurred at low GBMA (10° to 30°). The occurrence of twinning did not seem to have a clear relationship with GBMA.

4 Discussion

4.1 Activation of anomalous tension twins

The study revealed that under the conditions of hard orientation loading with various strain rates and grain sizes, adequate anomalous tension twins ($m<0$) in basal-textured Mg sheets were observed (Fig. 5(a)).

The m criterion in the present work and many other works is purely totally geometric, which

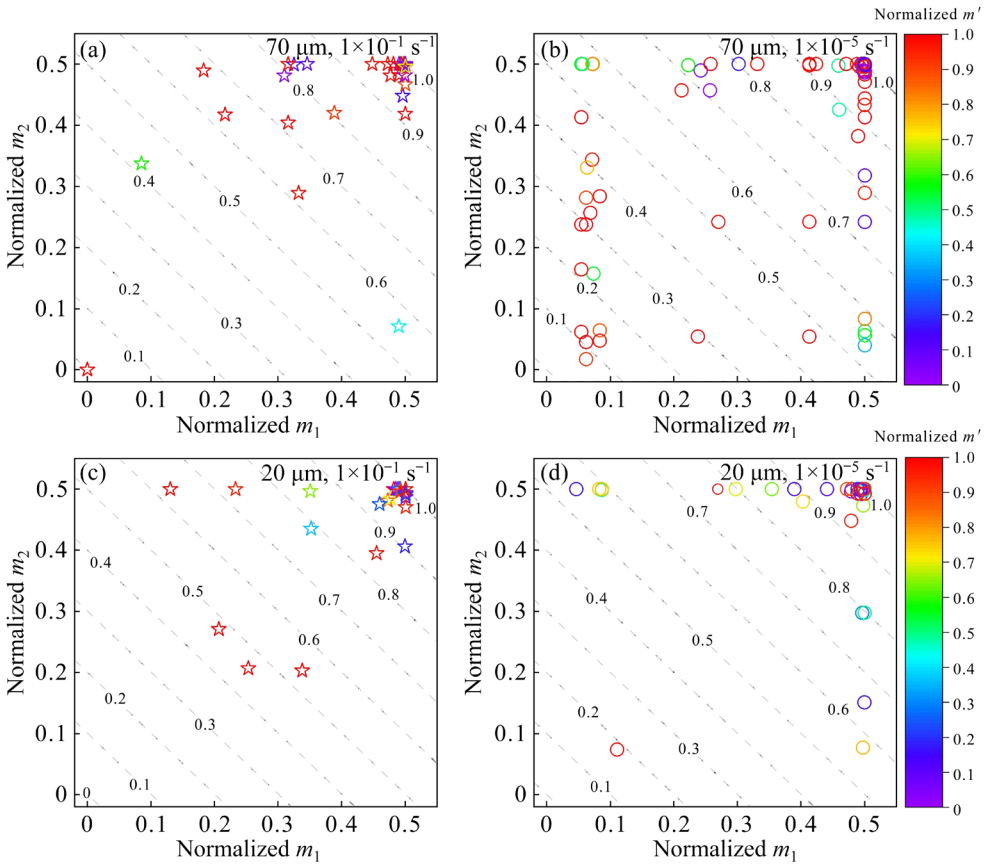

Fig. 9 Distributions of transmitted pairs in m'_{nor}–m_{nor1}–m_{nor2} heatmap for different grain sizes and strain rates

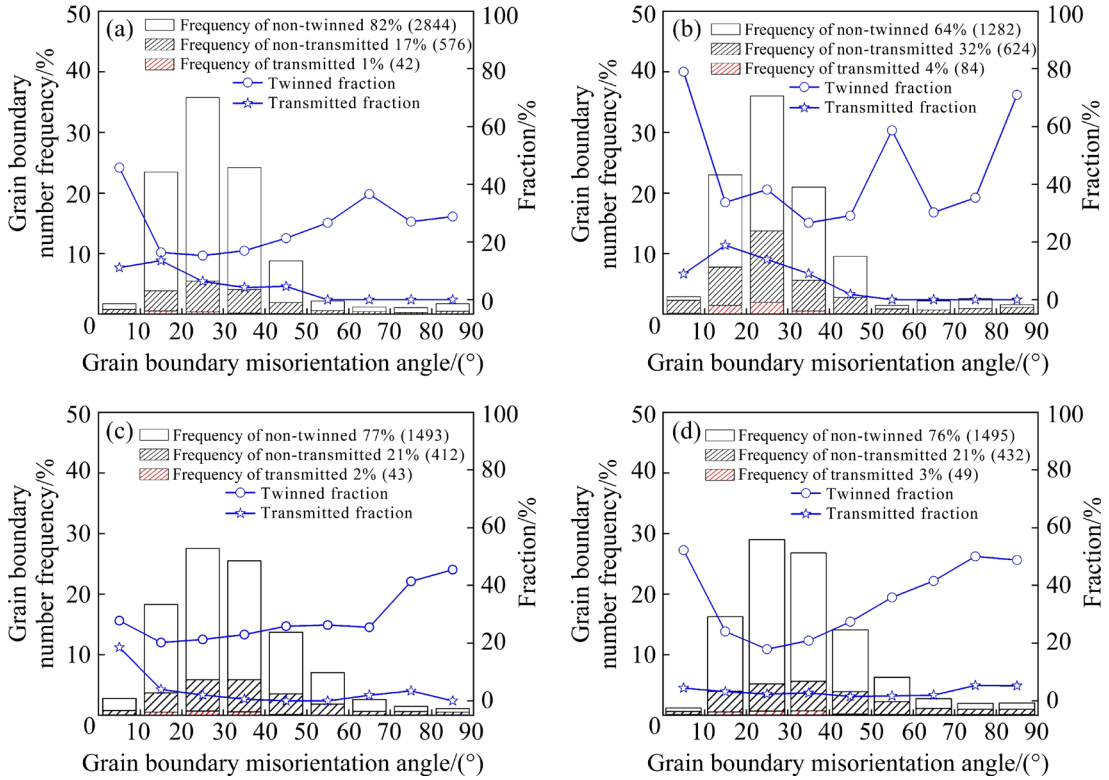

Fig. 10 Distributions of measured grain boundary misorientations and their ratios in pure Mg sheet for grain sizes of 70 μm (a, b) and 20 μm (c, d) at different strain rates: (a, c) 1×10^{-1} s^{-1}; (b, d) 1×10^{-5} s^{-1}

assumed that local stress coincided with global stress. However, it has been suggested that the abnormal behavior of anomalous twins ($m < 0$) may be caused by local stress fluctuation which may deviate from the global stress significantly. To verify this phenomenon, we employed EBSD to visualize (Fig. 11) and statistically analyze (Fig. 12) the deformation heterogeneity within normal and anomalous twins. Figure 11 shows the intragranular misorientation (IGM) and geometrically necessary dislocation (GND) density maps, the IPF maps of normal as well as anomalous twins with their parent grains, and a schematic representation of the twinning plane/directions of twins in the HCP cells. Homogeneous distribution of the IGM within the grains or higher IGM values in some regions within the grains at the twin boundaries of both normal and anomalous twins were observed (Fig. 11(c)). The long-range orientation gradient deformation heterogeneity was reflected in the IGM. The GND was necessary to maintain the strain compatibility of microstructures in the process of heterogeneous plastic deformation and was an important parameter for assessing the heterogeneity of plastic deformation. As shown in Fig. 11(d), higher GND density does not necessarily occur between normal and anomalous twins.

To ensure the statistical characteristics, Fig. 12 illustrates the distributions of grain orientation spread (GOS) and grain average GND density [36] for normal and anomalous twins and their parent grains in all samples. It should be noted that the magnitude of GND density between different grain sizes cannot be directly compared due to different EBSD step sizes (λ). It required conversion according to the relationship between the λ and GND density $\rho_{\mathrm{GND}}^{\mathrm{res}}$ [44] to unify GND density to the value at the same step size:

$$\rho_{\mathrm{GND}}^{\mathrm{res}}=\frac{\delta}{b\lambda} \tag{4}$$

where δ is the angular resolution of EBSD, and b is component of the Burgers vector. The statistical value distribution (Fig. 12) of GOS and grain average GND density were the same for normal and anomalous twins. Besides, the distributions of GOS and grain average GND density for the parent grains corresponding to normal and anomalous twins were not very different. Therefore, the IGM and GND density of normal and anomalous twins

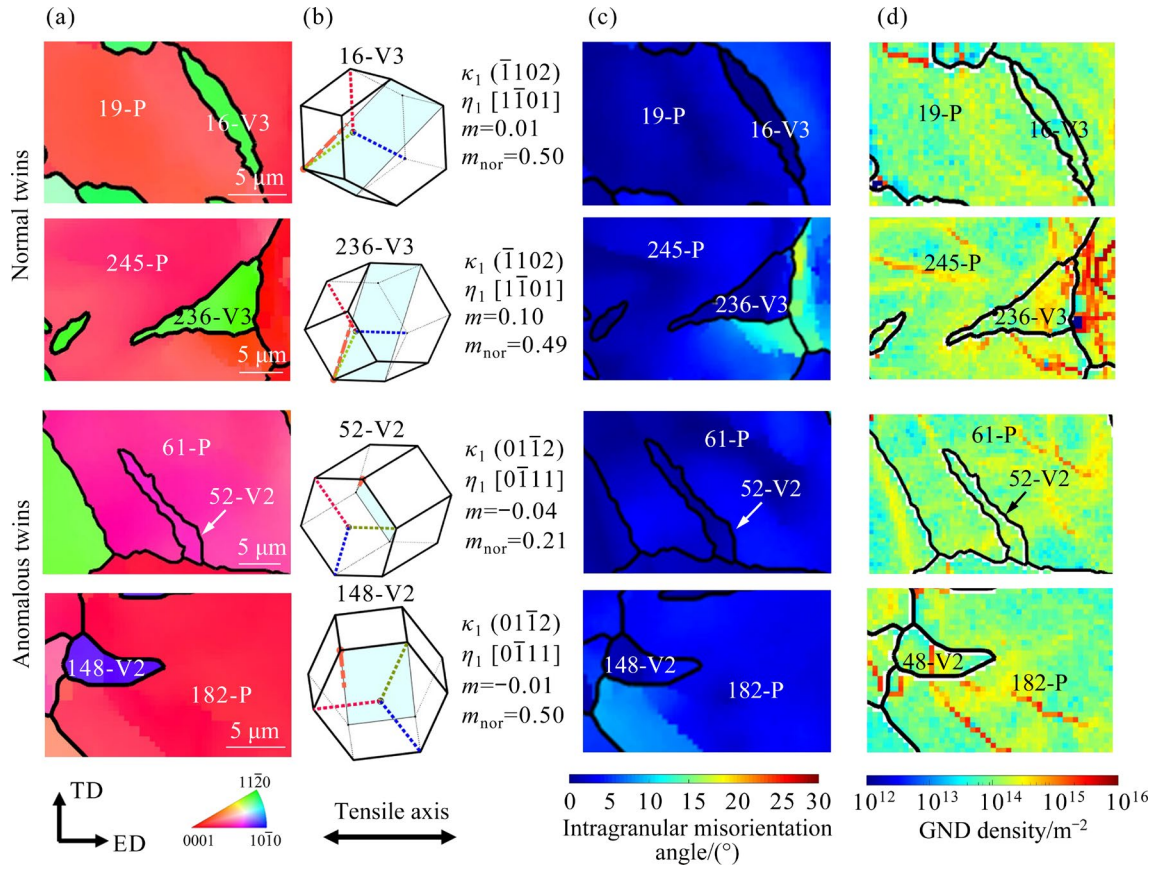

Fig. 11 (a) IPF maps; (b) Twinning plane κ_1, twinning direction η_1, and geometric parameters; (c, d) Corresponding IGM and GND density, respectively

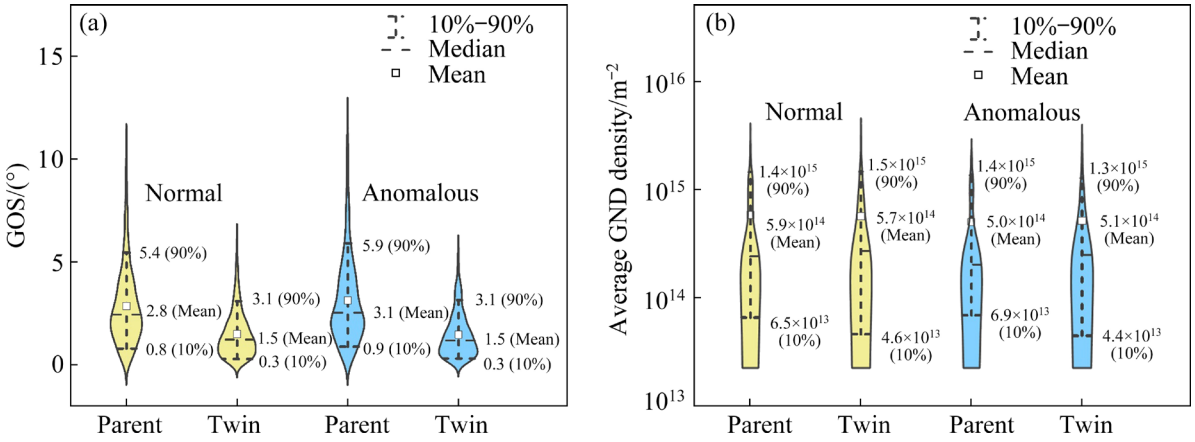

Fig. 12 Distributions of GOS (a) and average GND density (b) for all normal ($m > 0$) and anomalous ($m < 0$) twins and their parent grains

were the same at the grain scale. Above all, no essential relationship was found between anomalous twins and local deformation heterogeneity at grain scale.

As shown in Fig. 13, with the m values for prismatic slip in the parent grains increasing, the proportion of anomalous twins increased, suggesting that anomalous twins were more likely to be activated when the crystallographic orientation of the parent grains favored prismatic slip. The active anomalous twins in this context may be associated with coordinating the strain induced by prismatic slip. Similar hypotheses have been mentioned in some studies on Mg

alloys [27,33,45,46]. JONAS et al [27] observed the activation of numerous low m-value twin variants after room temperature tensile deformation of AZ31. They subsequently calculated the strain fields induced by slip/twinning and found that the large incompatible strains generated at grain boundaries during prismatic slip could be accommodated by activating low m-value twins. SHI et al [11] reported the occurrence of anomalous TTW during compression along the rolling direction (RD) in AZ31, with 23% of the TTW variants having low m-values. They suggested that these low m-value TTWs were activated to coordinate the prismatic slip and twinning in adjacent grains. KOIKE et al [46] found the activation of anomalous TTW in AZ31 after tension deformation along the RD and attributed the activation of anomalous TTW to the need to coordinate the strain generated by basal slip in parent grains when the basal slip activity within parent grains is higher than that in the adjacent grains. HUA et al [33] investigated the compression process along the ED in extruded Mg−3Y using quasi-in-situ SEM and EBSD and found the activation of anomalous twins. They also observed a good correlation between twinning activation and prismatic slip.

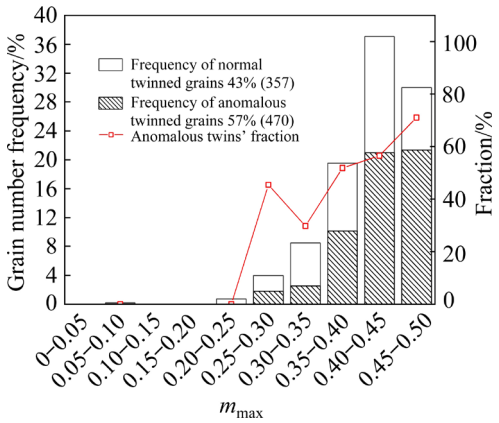

Fig. 13 Relation between anomalous twin ($m < 0$) fraction and Schmid factor of prismatic slip in corresponding grains

We did not find an inevitable relationship between anomalous twins and local deformation heterogeneity at grain scale, at least from the perspective of statistics. The local strain deviation from the globally applied stress was not the whole story, and it was more likely that the activation of anomalous twin was to coordinate the strain due to prismatic slip.

4.2 Parameters for determining twin transmission

In HCP metals, m' was one of the most frequently used parameters to assess the probability of twin transmission. However, we observed that ~20% of twin transmission pairs had negative m' values and ~50% of twin transmission pairs had low m' values ($m' < 0.75$) at different strain rates and grain sizes, which indicated that m' was not a good correlation of twin transmission behavior under the current hard orientation loading conditions. The result was similar to our previous works [24]. Similarly, when pure Mg was compressed along the RD, KUMAR et al [43] discovered the occurrence of twin transmission pairs with negative values of m' under soft orientation loading. Thus, when both m_{nor} and m'_{nor} values were taken into account, the m_{nor} or m'_{nor} was close to the maximum value for nearly all transmitted pairs (96%), whereas a single m or m' has some limitations and did not correlate well with the current twin transmission behavior under hard orientation loading conditions. Twin transmission was closely related to grain boundary, and transmitted pairs were more likely to occur at lower GBMAs (10°−30°) (Fig. 10). Other researches also obtained similar results [24,42,43,47,48]. According to KUMAR et al [43], the fraction of twin transmission was insensitive to the grain boundary orientation axis but diminished as the grain boundary orientation difference increased. As a result, it was important to consider grain boundary structure and local deformation coordination when making a correlation about the activation of anomalous twins and the behavior of twin transmission.

5 Conclusions

(1) A total of 1609 TTWs identified from 1693 twins were counted and analyzed. The activated twins after tension to fracture of pure Mg with different grain sizes under hard orientation loading conditions at different strain rates were all dominated by TTW; the m values of the activated twins were centrally distributed in the range of −0.2 to 0.2, and 51% of the anomalous twins ($m < 0$) occurred. Twin variant selection exhibited similar trends for samples with different grain sizes or strain rates. The m_{nor} values of twins were concentrated in 0.45−0.5, with 74% of twins exhibiting larger values ($m_{nor} > 0.4$), suggesting that

normalized m_{nor} could more effectively correlate with the twin variant selection. The active anomalous twins were correlated with the m values of prismatic slip in the parent grains, which meant that the local condition played a critical role in twinning behavior.

(2) Twin transmission was observed in ~343 transmitted twins out of 1609 total twins. For pure Mg under hard orientation loading conditions, the proportion of twin transmission increased with decreasing strain rate. About 50% of the transmitted twin pairs exhibited low m' values ($m' < 0.75$), and 20% of those occurred even negative values. From a statistical perspective, although single m and m' failed to correlate with the current twin transmission behavior under hard orientation loading conditions, combining m and m' could correlate well with twin transmission, with 96% of transmitted pairs having m_{nor} or m'_{nor} close to the maximum value. Twin transmission was more likely to occur at lower GBMA (10°−30°).

CRediT authorship contribution statement

Sai-jun HUANG: Writing − Original draft, Investigation, Formal analysis, Conceptualization, Visualization; **Ran NI:** Formal analysis, Writing − Review & editing; **You-fu WAN:** Investigation, Formal analysis; **Hao ZHOU** and **Ying ZENG:** Writing − Review & editing; **Dong-di YIN:** Conceptualization, Methodology, Supervision, Writing − Review & editing, Funding acquisition.

Declaration of competing interest

The authors declare that they have no known competing financial interests or personal relationships that could have appeared to influence the work reported in this paper.

Acknowledgments

This work was supported by the National Natural Science Foundation of China (Nos. 52171125, 52071178). We would like to thank the Analytical and Testing Center of Southwest Jiaotong University for assistance with SEM and EBSD characterization.

References

[1] LI Zi-han, ZHOU Guo-wei, LI Da-yong, WANG Hua-miao, TANG Wei-qin, PENG Ying-hong, ZUROB H S, WU Pei-dong. Crystal plasticity based modeling of grain boundary sliding in magnesium alloy AZ31B sheet [J]. Transactions of Nonferrous Metals Society of China, 2021, 31(1): 138−155.

[2] WANG Tong, ZHA Min, DU Chun-feng, JIA Hai-long, WANG Cheng, GUAN Kai, GAO Yi-peng, WANG Hui-yuan. High strength and high ductility achieved in a heterogeneous lamella-structured magnesium alloy [J]. Materials Research Letters, 2023, 11(3): 187−195.

[3] XIE Dong-sheng, PAN Hu-cheng, PAN Zhen, FU Tong, ZENG Zhuo-ran, XIE Hong-bo, REN Yu-ping, TANG Wei-neng, QIN Gao-wu. Achieving outstanding heat-resistant properties in Mg alloy via constructing stable solute-network [J]. Materials Research Letters, 2023, 11(5): 374−382.

[4] YANG Wu, QUAN Gao-feng, JI Bin, WAN You-fu, ZHOU Hao, ZHENG Jiang, YIN Dong-di. Effect of Y content and equal channel angular pressing on the microstructure, texture and mechanical property of extruded Mg−Y alloys [J]. Journal of Magnesium and Alloys, 2022, 10(1): 195−208.

[5] NI Ran, BOEHLERT C J, ZENG Ying, CHEN Bo, HUANG Sai-jun, ZHENG Jiang, ZHOU Hao, WANG Qu-dong, YIN Dong-di. Automated analysis framework of strain partitioning and deformation mechanisms via multimodal fusion and computer vision [J]. International Journal of Plasticity, 2024, 182: 104119.

[6] JIANG Zhi-wei, YIN Dong-di, WAN You-fu, NI Ran, ZHOU Hao, ZHENG Jiang, WANG Qu-dong. Operating slip modes and inhomogeneous plastic deformation of Mg−10Gd−3Y−0.5Zr alloy during compression [J]. Transactions of Nonferrous Metals Society of China, 2023, 33(1): 79−94.

[7] BIAN Nan, LI Feng, NIU Wen-tao, LI Chao, LI Yuan-qi. Dual strengthened control of recrystallization behavior on CVCDE magnesium alloy containing characteristic structure [J]. Acta Metallurgica Sinica (English Letters), 2023, 36: 1805−1821.

[8] CHRISTIAN J W, MAHAJAN S. Deformation twinning [J]. Progress in Materials Science, 1995, 39(1/2): 1−157.

[9] YAN Chang-jian, GUAN Bo, XIN Yun-chang, ZHAO Ling-yu, HUANG Guang-jie, HONG Rui, CHEN Xiao-bo, CHU P K. Mechanical and corrosion behavior of a biomedical Mg–6Zn–0.5Zr alloy containing a large number of twins [J] Acta Metallurgica Sinica (English Letters), 2023, 36: 439−455.

[10] ZHAO Ling-yu, ZHU Wei, ZHANG Chao, XIN Yun-chang, YAN Chang-jian, CHENG Yao, JIN Zhao-yang. Detwinning and anneal-hardening behaviors of pre-twinned AZ31 alloys under cryogenic loading [J] Acta Metallurgica Sinica (English Letters), 2024, 37: 1551−1563.

[11] SHI Zhang-zhi, ZHANG Yu-dong, WAGNER F, JUAN P A, BERBENNI S, CAPOLUNGO L, LECOMTE J S, RICHETON T. On the selection of extension twin variants with low Schmid factors in a deformed Mg alloy [J]. Acta Materialia, 2015, 83: 17−28.

[12] YOO M H. Slip, twinning, and fracture in hexagonal close-packed metals [J]. Metallurgical Transactions A, 1981, 12(3): 409−418.

[13] BETTLES C, BARNETT M. Advances in wrought magnesium alloys: Fundamentals of processing, properties and applications [M]. Cambridge: Woodhead Publishing, 2012.

[14] BARNETT M R. Twinning and the ductility of magnesium

alloys: Part I. “Tension” twins [J]. Materials Science and Engineering: A, 2007, 464(1/2): 1−7.

[15] BARNETT M R. Twinning and the ductility of magnesium alloys: Part II. “Contraction” twins [J]. Materials Science and Engineering: A, 2007, 464(1/2): 8−16.

[16] KNEZEVIC M, ZECEVIC M, BEYERLEIN I J, BINGERT J F, MCCABE R J. Strain rate and temperature effects on the selection of primary and secondary slip and twinning systems in HCP Zr [J]. Acta Materialia, 2015, 88: 55−73.

[17] ULACIA I, DUDAMELL N V, GÁLVEZ F, YI S B, PÉREZ-PRADO M T, HURTADO I. Mechanical behavior and microstructural evolution of a Mg AZ31 sheet at dynamic strain rates [J]. Acta Materialia, 2010, 58(8): 2988−2998.

[18] CHUN Y B, DAVIES C H J. Twinning-induced negative strain rate sensitivity in wrought Mg alloy AZ31 [J]. Materials Science and Engineering: A, 2011, 528(18): 5713−5722.

[19] SHI Dong-feng, PÉREZ-PRADO M T, CEPEDA-JIMÉNEZ C M. Effect of solutes on strength and ductility of Mg alloys [J]. Acta Materialia, 2019, 180: 218−230.

[20] XIN Ren-long, LIANG Ying-chun, DING Chang-hong, GUO Chang-fa, WANG Bing-shu, LIU Qing. Geometrical compatibility factor analysis of paired extension twins in extruded Mg−3Al−1Zn alloys [J]. Materials & Design, 2015, 86: 656−663.

[21] HONG S G, PARK S H, LEE C S. Role of $\{10\bar{1}2\}$ twinning characteristics in the deformation behavior of a polycrystalline magnesium alloy [J]. Acta Materialia, 2010, 58(18): 5873−5885.

[22] BEYERLEIN I J, MCCABE R J, TOMÉ C N. Effect of microstructure on the nucleation of deformation twins in polycrystalline high-purity magnesium: A multi-scale modeling study [J]. Journal of the Mechanics and Physics of Solids, 2011, 59(5): 988−1003.

[23] MU Si-jia, JONAS J J, GOTTSTEIN G. Variant selection of primary, secondary and tertiary twins in a deformed Mg alloy [J]. Acta Materialia, 2012, 60(5): 2043−2053.

[24] CHAI Yan-qin, BOEHLERT C J, WAN You-fu, HUANG Guang-hao, ZHOU Hao, ZHENG Jiang, WANG Qu-dong, YIN Dong-di. Anomalous tension twinning activity in extruded Mg sheet during hard-orientation loading at room temperature [J]. Metallurgical and Materials Transactions A, 2021, 52: 449−456.

[25] KUMAR M A, BEYERLEIN I J. Local microstructure and micromechanical stress evolution during deformation twinning in hexagonal polycrystals [J]. Journal of Materials Research, 2020, 35(3): 217−241.

[26] BEYERLEIN I J, KUMAR M A. The stochastic nature of deformation twinning: Application to HCP materials [M]. Cham: Springer International Publishing, 2018.

[27] JONAS J J, MU Si-jia, AL-SAMMAN T, GOTTSTEIN G, JIANG Lan, MARTIN Ė. The role of strain accommodation during the variant selection of primary twins in magnesium [J]. Acta Materialia, 2011, 59(5): 2046−2056.

[28] WANG Fu-lin, SANDLÖBES S, DIEHL M, SHARMA L, ROTERS F, RAABE D. In situ observation of collective grain-scale mechanics in Mg and Mg−rare earth alloys [J]. Acta Materialia, 2014, 80: 77−93.

[29] NAVE M D, BARNETT M R. Microstructures and textures of pure magnesium deformed in plane-strain compression [J]. Scripta Materialia, 2004, 51(9): 881−885.

[30] HUANG Guang-hao, YIN Dong-di, LU Jia-wei, ZHOU Hao, ZENG Ying, QUAN Gao-feng, WANG Qu-dong. Microstructure, texture and mechanical properties evolution of extruded fine-grained Mg−Y sheets during annealing [J]. Materials Science and Engineering: A, 2018, 720: 24−35.

[31] LU Jia-wei, YIN Dong-di, HUANG Guang-hao, QUAN Gao-feng, ZENG Ying, ZHOU Hao, WANG Qu-dong. Plastic anisotropy and deformation behavior of extruded Mg−Y sheets at elevated temperatures [J]. Materials Science and Engineering: A, 2017, 700: 598−608.

[32] YIN Dong-di, BOEHLERT C J, LONG Li-jun, HUANG Guang-hao, ZHOU Hao, ZHENG Jiang, WANG Qu-dong. Tension-compression asymmetry and the underlying slip/twinning activity in extruded Mg−Y sheets [J]. International Journal of Plasticity, 2021, 136: 102878.

[33] HUA Shen, JIANG Zhi-wei, WAN You-fu, HUANG Guang-hao, ZHOU Hao, ZHENG Jiang, WANG Qu-dong, YIN Dong-di. A statistical analysis of compressive deformation mechanisms in an extruded Mg−3Y sheet [J]. Materials Science and Engineering: A, 2021, 825: 141927.

[34] CHAI Yan-qin, YIN Dong-di, HUA Shen, HUANG Guang-hao, ZHOU Hao, ZHENG Jiang, WANG Qu-dong. Role of yttrium content in twinning behavior of extruded Mg−Y sheets under tension/compression [J]. Transactions of Nonferrous Metals Society of China, 2022, 32(11): 3534−3549.

[35] NI Ran, JIANG Zhi-wei, YIN Dong-di, YANG Wu, ZHOU Hao, ZHENG Jiang, WANG Qu-dong. Investigation on slip activity and plastic heterogeneity of aged Mg−10Y sheets during compression [J]. Metallurgical and Materials Transactions A, 2022, 53: 535−555.

[36] NI Ran, MA Shi-jun, LONG Li-jun, ZHENG Jiang, ZHOU Hao, WANG Qu-dong, YIN Dong-di. Effects of precipitate on the slip activity and plastic heterogeneity of Mg−11Y−5Gd−2Zn−0.5Zr (wt.%) during room temperature compression [J]. Materials Science and Engineering: A, 2021, 804: 140738.

[37] HIELSCHER R, SILBERMANN C B, SCHMIDL E, IHLEMANN J. Denoising of crystal orientation maps [J]. Journal of Applied Crystallography, 2019, 52: 984−996.

[38] BACHMANN F, HIELSCHER R, SCHAEBEN H. Texture analysis with MTEX-free and open source software toolbox [J]. Solid State Phenomena, 2010, 160: 63−68.

[39] YIN Dong-di, CHEN Bo, CHAI Yan-qin, WAN You-fu, ZHOU Hao, ZHENG Jiang, WANG Qu-dong, ZENG Ying. Statistical investigation of deformation mechanisms in rolled Mg sheet during compression [J]. Transactions of Nonferrous Metals Society of China, 2023, 33(10): 2970−2985.

[40] LUSTER J, MORRIS M A. Compatibility of deformation in two-phase Ti−Al alloys: Dependence on microstructure and orientation relationships [J]. Metallurgical & Materials Transactions A, 1995, 26: 1745−1756.

[41] KUMAR M A, BEYERLEIN I J, MCCABE R J, TOMÉ C N. Grain neighbour effects on twin transmission in hexagonal close-packed materials [J]. Nature Communications, 2016,

7(1): 13826−13835.
[42] BEYERLEIN I J, CAPOLUNGO L, MARSHALL P E, MCCABE R J, TOMÉ C N. Statistical analyses of deformation twinning in magnesium [J]. Philosophical Magazine, 2010, 90(16): 2161−2190.
[43] KUMAR M A, MCCABE R J, TAUPIN V, TOMÉ C N, CAPOLUNGO L. Statistical characterization of twin transmission across grain boundaries in magnesium [J]. Materials Characterization, 2022, 194: 112457.
[44] ZHU Chao-yi, HARRINGTON T, LIVESCU V, GRAY G T, VECCHIO K S. Determination of geometrically necessary dislocations in large shear strain localization in aluminum [J]. Acta Materialia, 2016, 118: 383−394.
[45] WANG Xiao-xia, MAO Ping-li, LIU Zheng, WANG Zhi, WANG Feng, ZHOU Le, WEI Zi-qi. Nucleation and growth analysis of $\{10\bar{1}2\}$ extension twins in AZ31 magnesium alloy during in-situ tension [J]. Journal of Alloys and Compounds, 2020, 817: 152967.
[46] KOIKE J, SATO Y, ANDO D. Origin of the anomalous $\{10\bar{1}2\}$ twinning during tensile deformation of Mg alloy sheet [J]. Materials Transactions, 2008, 49(12): 2792−2800.
[47] HONG Xia, GODFREY A, LIU Wei. Challenges in the prediction of twin transmission at grain boundaries in a magnesium alloy [J]. Scripta Materialia, 2016, 123: 77−80.
[48] KUMAR M A, CAPOLUNGO L, MCCABE R J, TOMÉ C N. Characterizing the role of adjoining twins at grain boundaries in hexagonal close packed materials [J]. Scientific Reports, 2019, 9(1): 3846.

不同晶粒尺寸和应变速率下纯镁板材反常孪晶和孪晶转移的统计分析

黄赛君[1]，倪 然[1]，万有富[1]，周 浩[2]，曾 迎[1]，尹冬弟[1]

1. 西南交通大学 材料科学与工程学院 材料先进技术教育部重点实验室，成都 610031；
2. 南京理工大学 材料科学与工程学院 纳米异构材料中心，南京 210094

摘 要：对晶粒尺寸为 70 和 20 μm 的强基面织构纯镁板材以应变速率 1×10^{-1} 和 1×10^{-5} s^{-1} 沿硬取向拉伸至断裂后的孪晶行为进行统计分析。观察到 1609 例拉伸孪晶，包含大量(~51%)反常孪晶(Schmid 因子 m<0)，晶粒尺寸和应变速率对孪晶变体选择没有显著影响。大多数孪晶变体(74%)与提出的归一化 m(m_{nor})表现出良好的相关性。孪晶转移与 Luster−Morris 参数 (m') 没有很好的相关性，然而大多数孪晶转移(96%)都表现出较大的归一化 m 和 m' (m'_{nor})值。当晶界取向差较低(10°~30°)时，孪晶转移的比例增加。反常孪晶的激活与柱面滑移的 m 有很好的相关性。基于统计性分析，提出相较于广泛使用的几何参数 m 和 m'，m_{nor} 和 m'_{nor} 与反常孪晶具有更好的相关性，局部变形协调对反常孪晶激活起着重要作用。

关键词：镁；反常孪晶；孪晶转移；Schmid 因子；Luster−Morris 参数

(Edited by Xiang-qun LI)